

# Hybrid optical–electrical detection of donor electron spins with bound excitons in silicon

C. C. Lo<sup>1,2,\*</sup>, M. Urdampilleta<sup>1</sup>, P. Ross<sup>1</sup>, M. F. Gonzalez-Zalba<sup>3</sup>, J. Mansir<sup>1</sup>, S. A. Lyon<sup>4</sup>, M. L. W. Thewalt<sup>5</sup>, and J. J. L. Morton<sup>1,2</sup>

<sup>1</sup>London Centre for Nanotechnology, University College London, London WC1H 0AH, U.K.

<sup>2</sup>Department of Electronic and Electrical Engineering, University College London, London WC1E 7JE, U.K.

<sup>3</sup>Hitachi Cambridge Laboratory, J. J. Thomson Avenue, Cambridge CB3 0HE, U.K.

<sup>4</sup>Department of Electrical Engineering, Princeton University, Princeton, New Jersey 08544, USA. and

<sup>5</sup>Simon Fraser University, Burnaby, British Columbia V5A 1S6, Canada.

## I. SHIFTS IN D<sup>0</sup>X TRANSITION ENERGIES DUE TO TEMPERATURE

Fluctuations in sample temperature can affect the donor bound exciton transition energies. Figure 1 shows the electrically-detected zero-magnetic field D<sup>0</sup>X spectrum as a function of cryostat temperature. At higher temperatures, a red shift occurs due to the temperature-dependent silicon bandgap. We fit the variation to temperature with the form [1]:  $\Delta E[T] = E_0 - AT^P$ , with  $A = 0.1 \pm 0.03 \mu\text{eV}$  and  $P = 2 \pm 0.2$ . We note that these temperature-dependent variations in transition energies are small compared with those caused by typical strains in silicon devices.

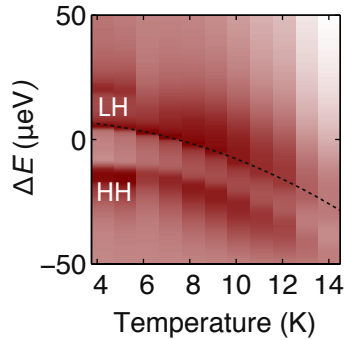


FIG. 1. Temperature dependence of D<sup>0</sup>X transition energies measured by electrical detection with  $B = 0$  T. The dashed line is fit to data, see text for details.

## II. D<sup>0</sup>X $g$ -FACTORS

The bound exciton  $g$ -factors can be calculated by assuming for the hole states:

$$H_B = \mu_B [g'_1(\mathbf{J} \cdot \mathbf{B}) + g'_2(\mathbf{J}^3 \cdot \mathbf{B})] \quad (1)$$

Where  $g'_1$  and  $g'_2$  are the isotropic and anisotropic terms, respectively, and the ' emphasize that the D<sup>0</sup>X hole states have a different  $g$ -factors from free valence band or acceptor hole states. In this case  $B \parallel \hat{n}$ , where  $\hat{n}$  is the normal of the silicon substrate along the  $\langle 100 \rangle$  crystallographic direction, the  $g$ -factors simplify to  $g_{LH} = g'_1 + \frac{1}{4}g'_2$  for the light hole  $J = 1/2$  states, and  $g_{HH} = g'_1 + \frac{9}{4}g'_2$  for the heavy hole  $J = 3/2$  states. We assume an isotropic  $g_d = 1.9985$  for the phosphorus donor electrons, and from the measured spectra, we extract the bound exciton hole-state  $g$ -factors to be  $g_{LH} = 0.86$  and  $g_{HH} = 1.33$  in this magnetic field orientation, with corresponding  $g'_1 = 0.80$  and  $g'_2 = 0.24$ , in agreement with earlier bound exciton measurements [2].

\* cheuk.lo@ucl.ac.uk.

### III. D<sup>0</sup>X IONIZATION TIME

The D<sup>0</sup>X ionization rate can be estimated from Einstein's coefficient for absorption, as:

$$\dot{n}_1 = -(B_{12}u_\nu) n_1, \quad (2)$$

where  $n_1$  is the ground state (neutral donor) population,  $B_{12}$  Einstein's absorption coefficient, and  $u_\nu$  the spectral energy density of the laser. The oscillator strength of the D<sup>0</sup>X transition for all shallow donors is  $f \approx 10^{-5}$  [3], which is related to  $B_{12}$  by:

$$B_{12} = \left( \frac{q^2}{4\epsilon_0 m_e h\nu} \right) \frac{1}{f} \approx 4.4 \times 10^{16} \text{ m}^3/\text{Js}^2 \quad (3)$$

where  $\epsilon_0$  is the vacuum permittivity,  $m_e$  the electron mass,  $h\nu \approx 1.15$  eV the optical transition energy, and  $q$  the elementary charge. The spectral energy density of the excitation is given by:

$$u_\nu = \left( \frac{4\pi}{c} \right) \frac{I}{\Delta\nu} \quad (4)$$

where  $c$  is the speed of light,  $I$  the laser intensity, and  $\Delta\nu$  the laser line width. For our fiber laser with  $\Delta\nu \approx 70$  kHz, and the experimentally used laser intensity of  $I \approx 3$  mW/mm<sup>2</sup>, the spectral energy density is  $u_\nu \approx 2 \times 10^{-9}$  J/m<sup>3</sup>Hz. Therefore, the estimated transition rate is  $B_{12}u_\nu \approx 85$  MHz, which is much faster than the spin relaxation time of  $T_1 \approx 10$  s for shallow donors in liquid helium temperatures [4].

### IV. ESTIMATION OF ELECTRON SPIN POLARIZATION

The measured ESR echo intensity is directly proportional to the electron spin polarization:  $y \propto P$ . At thermal equilibrium, the electron spin polarization is given by  $P_0 = \tanh(g_d\mu_B B/2k_B T)$ , where  $g_d = 1.9985$  is the phosphorus donor  $g$ -factor,  $\mu_B$  the Bohr magneton and  $k_B$  the Boltzmann constant. At the experimental conditions of  $B = 0.35$  T and  $T = 4.3$  K, the donor electron spin polarization is  $P_0 = 5.5\%$ . The ratio of the ESR echo intensities would then give the hyperpolarized electron spin polarization:  $P = P_0 \times (y/y_0)$ . Cross-relaxation of phosphorus donors with the other nuclear spin state ( $m_I = +1/2$ ) is negligible in these time scales given the temperature and magnetic fields used, and the nuclear spin polarization in our experiments is essentially zero. Hence, the maximum achievable echo intensity change will be  $(y/y_0) \approx 18$ , corresponding to 100% electron spin polarization of the donor electron. The nuclear spin states can eventually acquire significant polarization with prolonged laser excitation, or with appropriate RF and microwave pulses to transfer the hyperpolarized electron spin state to the nuclear spin, resulting in echo intensities greater than the near 100% polarization shown in the main text.

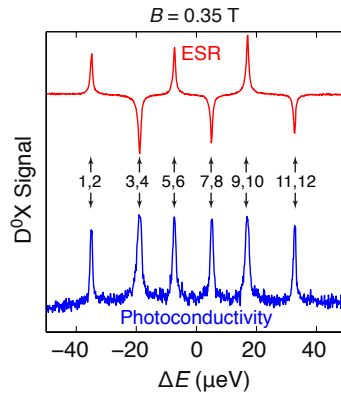


FIG. 2. ESR echo (red) and contactless photoconductivity (blue) detected laser sweep for D<sup>0</sup>X for bulk P-doped ( $10^{14}$  cm<sup>-3</sup>) <sup>28</sup>Si. The laser sweep is centered at 1.149,849 eV and measured at 4.3 K. The traces are normalized and offset for clarity.

Antipolarization (negative electron spin polarization) can be achieved by tuning the laser to excite the spin down electronic states, resulting in a sign reversal of the ESR echo. This effect is shown in figure 2, where we monitor the donor spin echo intensity while sweeping the bound exciton laser to cover all relevant transitions. We also show the contactless bulk photoconductivity measurements detected simultaneously, and the corresponding transitions are as indicated.

## V. SHIFTS IN D<sup>0</sup>X TRANSITION ENERGIES DUE TO STRAIN

The strain dependence of bound excitons under uniaxial strain have previously been calculated for acceptors in silicon, where the coupling parameters and relevant deformation potentials were found by fitting to experimental data [5, 6]. Here, we use a single-particle perturbative approach to model the strain dependence of bound excitons of shallow donors, and we extract the relevant deformation potentials from experimental data for phosphorus donors ( $\alpha_1$  transitions in figure 1 of reference [7]).

The donor bound exciton consists of two electrons and one hole residing at the donor site. The two electrons occupy the donor electron  $A$  ( $\Gamma_1$ ) sub-level of the 1s ground state, forming a spin-0 singlet. In the first order approximation, we consider only the perturbations to the single-particle electron ( $E_{d,0}$ ) and hole ( $E_h$ ) states induced by strain:

$$\Delta E_{D^0X}(\epsilon) \approx \Delta E_d(\epsilon) - \Delta E_h(\epsilon) \quad (5)$$

where  $\epsilon$  is the conventional  $3 \times 3$  strain tensor, and our calculations can easily be applied in conjunction with semiconductor processing simulators to estimate the strain-induced D<sup>0</sup>X shifts in silicon devices. Stress and strain tensors are related by the stiffness coefficients, and we use  $C_{11} = 166$  GPa,  $C_{12} = 63.9$  GPa, and  $C_{44} = 79.6$  GPa [8].

The neutral donor 1s ground state energies can be calculated by taking valley-orbit splitting into account in the valley basis  $\{+X, -X, +Y, -Y, +Z, -Z\}$ . In the unstrained case, the Hamiltonian is given by:

$$H_{d,0} = \begin{bmatrix} E_0 & \Delta_1 & \Delta_2 & \Delta_2 & \Delta_2 & \Delta_2 \\ \Delta_1 & E_0 & \Delta_2 & \Delta_2 & \Delta_2 & \Delta_2 \\ \Delta_2 & \Delta_2 & E_0 & \Delta_1 & \Delta_2 & \Delta_2 \\ \Delta_2 & \Delta_2 & \Delta_1 & E_0 & \Delta_2 & \Delta_2 \\ \Delta_2 & \Delta_2 & \Delta_2 & \Delta_2 & E_0 & \Delta_1 \\ \Delta_2 & \Delta_2 & \Delta_2 & \Delta_2 & \Delta_1 & E_0 \end{bmatrix} \quad (6)$$

where all parameters are found by fitting to the experimentally determined 1s ground state splittings. For the strain-induced shifts to the donor energy ground state, we use valley repopulation as formulated by Wilson and Feher [9]. The 6-fold degenerate conduction band minima along the equivalent [100] directions shift with strain according to the deformation potentials [8]:

$$H_{CB}(\epsilon) = \Xi_d \text{Tr}\{\epsilon\} + \Xi_u \begin{bmatrix} \epsilon_{11} & 0 & 0 & 0 & 0 & 0 \\ 0 & \epsilon_{11} & 0 & 0 & 0 & 0 \\ 0 & 0 & \epsilon_{22} & 0 & 0 & 0 \\ 0 & 0 & 0 & \epsilon_{22} & 0 & 0 \\ 0 & 0 & 0 & 0 & \epsilon_{33} & 0 \\ 0 & 0 & 0 & 0 & 0 & \epsilon_{33} \end{bmatrix} \quad (7)$$

where  $\epsilon_{ii}$  are the diagonal components of  $\epsilon$ . These shifts in valley energies cause the donor state to “repopulate” to the lower lying valleys. To calculate the donor ground state energy as a consequence of this valley repopulation effect, we solve the total Hamiltonian for  $\Delta E_d(\epsilon)$  by combing the donor valley-orbit and conduction band deformation potential Hamiltonians:

$$H_d(\epsilon) = H_{d,0} + H_{CB}(\epsilon) \quad (8)$$

For the valence band at the  $\Gamma_8$  point, we use the Pikus-Bir Hamiltonian to describe the strain-induced interactions of the the  $|J, m_j\rangle = |3/2, \pm 1/2\rangle$  (light hole) and  $|J, m_j\rangle = |3/2, \pm 3/2\rangle$  (heavy hole) bands [8]:

$$H_h(\epsilon) = a' \text{Tr}\{\epsilon\} + b' \sum_{i=x,y,z} \left( J_i^2 - \frac{J^2}{3} \right) \epsilon_{ii} + \frac{d'}{\sqrt{3}} \sum_{i \neq j} (J_i J_j + J_j J_i) \epsilon_{ij} \quad (9)$$

Parameter	Symbol	Fitted value	Reference value
Hydrostatic DP	$a''$	-3.2 eV	-10 eV (Bulk band structure) [8]
CB DP	$\Xi_u$	15.5 eV	8.77 eV (Bulk band structure) [8]
VP DP	$b'$	-1.7 eV	-2.2 eV (Bulk band structure) [8]
	$d'$	-5.1 eV	-5.2 eV (Bulk band structure) [8]
P donor with VO	$E_0$		-35.4 meV [10]
	$\Delta_1$		-1.51 meV [10]
	$\Delta_2$		-2.17 meV [10]

TABLE I. Parameters used for the strain-induced shifts for the  $D^0X$  transitions. DP: Deformation potential. CB: Conduction band. VB: Valence band. VO: Valley-Orbit splitting.

Shifts to the valence band,  $\Delta E_h(\epsilon)$ , is found by solving the above Hamiltonian.

The contributions from the conduction band  $\Xi_d$  and valence band  $a'$  terms cannot be independently distinguished when fitting to experimental data, as they both correspond to the hydrostatic component of strain. Hence, we only use one fitting parameter,  $a''$ , to represent this component. A least-square fit to the experimental data for all three uniaxially strained directions ( $\langle 100 \rangle$ ,  $\langle 110 \rangle$ , and  $\langle 111 \rangle$ ) in reference [7] is used to obtain the values for the effective  $D^0X$  deformation potentials shown in table I.

We calculate the strain tensor components of the silicon nano-device structure with aluminum gate using COMSOL Multiphysics. The simulation is divided into two steps: (i) The 5 nm silicon dioxide and the silicon substrate are assumed to be strain-free at the oxidation temperature, which we set to be 900°C. Strain builds up when the oxidized substrate is cooled down to room temperature, which we take into account by using temperature-dependent thermal expansion coefficients. (ii) The aluminum gate is then introduced to the structure, assuming it to be strain-free when deposited. The simulation temperature is then ramped down to 4.2 K, again using temperature-dependent thermal expansion coefficients. The simulated strain profiles are shown in figure 3, and these components are used to calculate the bound exciton transition energies as described above.

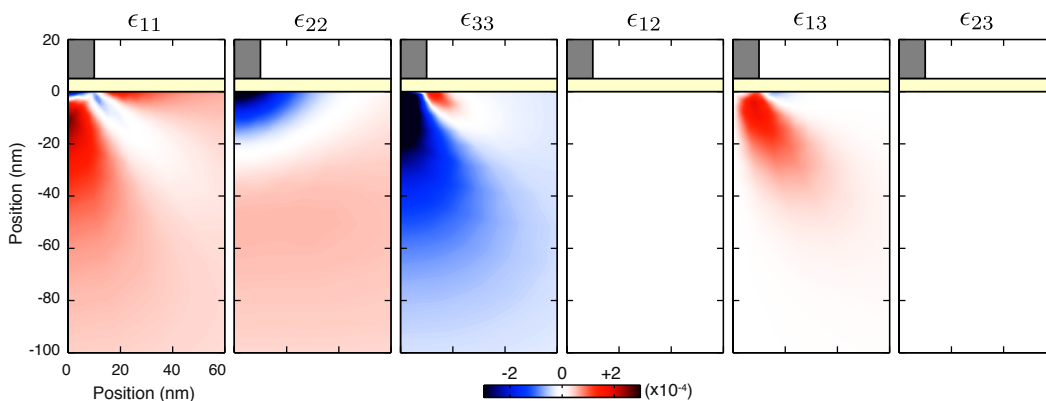


FIG. 3. Strain components due to thermal expansion coefficient mismatch in close proximity to aluminum gates at 4.2 K.

[1] M. Cardona, T. A. Meyer, and M. L. W. Thewalt. Temperature dependence of the energy gap of semiconductors in the low-temperature limit. *Physical Review Letters*, 92(19):196403, 2004.

[2] A. S. Kaminskii, V. A. Karasyuk, and Ya. E. Pokrovskii. Luminescence of excitons bound to phosphorus atoms in silicon subjected to a magnetic field. *Sov. Phys. JETP*, 52:211, 1980.

[3] P. J. Dean, W. F. Flood, and G. Kaminsky. Absorption due to bound excitons in silicon. *Physical Review*, 163(3):721, 1967.

[4] A. M. Tyryshkin, S. Tojo, J. J. L. Morton, H. Riemann, N. V. Abrosimov, P. Becker, H. J. Pohl, T. Schenkel, M. L. W.

- Thewalt, K. M. Itoh, and S. A. Lyon. Electron spin coherence exceeding seconds in high-purity silicon. *Nature Materials*, 11(2):143, 2012.
- [5] V. A. Karasyuk, A. G. Steele, A. Mainwood, D. M. Brake, and M. L. T. Thewalt. Ultrahigh-resolution photoluminescence studies of excitons bound to boron in silicon under uniaxial stress. *Physical Review B*, 45:11736, 1992.
- [6] V. A. Karasyuk, M. L. T. Thewalt, S. An, and E. C. Lightowers. Fourier-transform photoluminescence spectroscopy of excitons bound to group-iii acceptors in silicon: Uniaxial stress. *Physical Review B*, 56:15672, 1997.
- [7] M L. W. Thewalt and J. A. Rostworowski. Multiexciton complexes bound to phosphorus in silicon. *Physical Review Letters*, 41:808, 1978.
- [8] P. Y. Yu and M. Cardona. *Fundamentals of semiconductors - Physics and materials properties*, 3<sup>rd</sup> edition. Springer-Verlag, Berlin, Germany, 2001.
- [9] D. K. Wilson and G. Feher. Electron spin resonance experiments on donors in silicon. III. Investigation of excited states by the application of uniaxial stress and their importance in relaxation processes. *Physical Review*, 124(4):1068, 1961.
- [10] M. Friesen. Theory of the stark effect for p donors in si. *Physical Review Letters*, 94:186403, 2005.